Effects of complexing agents on electrochemical deposition of FeS_xO_y thin films

Aizuddin Supee[1,2]*, and Masaya Ichimura[2]

[1]*Faculty of Chemical and Energy Engineering, Universiti Teknologi Malaysia, 81310 Johor Bahru, Johor, Malaysia*

[2]*Department of Engineering Physics, Electronics and Mechanics, Nagoya Institute of Technology, Gokiso, Showa, Nagoya 466-8555, Japan*

E-mail: aizuddin@utm.my

FeS_xO_y thin films were deposited on indium-tin-oxide (ITO)-coated glass substrate at 15 ºC via galvanostatic electrochemical deposition from an aqueous solution containing 100 mM $Na_2S_2O_3$ and 30 mM $FeSO_4$. The effects of L(+)-tartaric acid ($C_4H_4O_6$) and lactic acid ($CH_3CH(OH)COOH$) under different concentration were investigated. All the deposited films were amorphous. With the complexing agents, the thickness was increased, and oxygen content was reduced significantly compared with the sample deposited without the complexing agents. In the photoelectrochemical measurement, p-type conductivity was confirmed. The photoresponsivity was not influenced significantly by the complexing agent, suggesting that the oxygen content does not drastically affect the properties of the deposited films probably because the local bonding configuration around Fe atoms in FeS_xO_y is similar to that in FeS_2.

1. Introduction

Growing interest in replacing a higher cost conventional silicon-based material in solar cell application exhibits that iron pyrite (FeS_2) has become one of the alternative materials widely chosen by many researchers.[1-3)] FeS_2 is a semiconductor which has remarkably large optical absorption coefficient ($\alpha > 10^5$ cm^{-1}) in the visible range[4-5)] and band gap energy around 0.95 eV,[4, 6)] and the theoretical conversion efficiency of a FeS_2-based solar cell is up to 20 %.[7)] In addition, Fe and S elements are extremely abundant in nature, cheap and nontoxic.

To date, FeS_2 thin films were fabricated by various methods such as spray pyrolysis,[8-9)] sulfurization of iron films,[10-11)] magnetron sputtering,[12-13)] metal organic chemical vapour deposition,[14-15)] chemical bath deposition (CBD),[16)] sol-gel,[17-18)] and electrochemical deposition (ECD).[3, 19-21)] Among them, ECD has the advantage of being economic, capable of large scale deposition and easy to control the films properties through electrochemical parameters.

Complexing agents are commonly used in solution deposition processes, and they are expected to improve electrolyte stability, produce sufficient adherence and smooth microstructure. For the CBD process, Vedavathi et al. found that FeS_2 films deposited using 0.1 M ethylenediaminetetraacetic (acid-EDTA) and 10-14 M ammonia were crystalline and that at 14 M ammonia, a pure pyrite phase with better surface morphology and lower film resistivity were obtained.[22)] Kassim et al.[23)] concluded that with increasing sodium tartrate concentration (0.1-0.3 M), the number of the FeS peaks in the X-ray diffraction results were reduced, the absorbance decreased, and the number of grains decreased. In the successive ionic layer adsorption and reaction method, Manikandan et al.[24)] claimed that the triethanolamine presence in the precursor solution resulted in a hexagonal shape of the crystalline structure in FeS_2 films.

So far, there is no work reported on the effects of complexing agents in iron sulfide films deposited by ECD. Thus, we carried out the ECD of iron sulfide under different concentration of tartaric acid ($C_4H_6O_6$) and lactic acid ($CH_3CH(OH)COOH$). Both chemicals have been successfully used to control composition and morphology in ECD of sulfides.[25-27)] In our previous work, it was shown that as-deposited iron sulfide films were

amorphous and included significant amount of oxygen.[1)] Thus the deposit is denoted by FeS_xO_y. The FeS_xO_y film deposited without complexing agents was set as the control sample, and the effects of different concentrations of complexing agents were investigated in terms of cyclic voltammetry, thickness, surface morphology, composition ratio, crystallinity, optical transmission, and photoresponse. As shown below, the oxygen content in deposited films was significantly reduced by adding the complexing agents. We discuss the influence of oxygen on the properties of iron sulfide by comparing between the control FeS_xO_y sample and the films deposited with the complexing agents.

2. Experimental methods

ECD was performed via galvanostatic ($I = -2.0$ mA/cm^2) mode at 15 ºC for 1.5 minutes. The deposition area was set to 1 cm^2 by masking. A 10 Ω/cm^2 indium-tin-oxide (ITO)-coated glass substrate, a platinum sheet, and a saturated calomel electrode (SCE) were used for the working electrode (WE), the counter electrode (CE), and the reference electrode (RE), respectively. The basic electrolyte solution contained 100 mM $Na_2S_2O_3$ and 30 mM $FeSO_4$ for the control sample,[1)] and different concentrations of tartaric acid (5-50 mM), and lactic acid (56-167 mM) were added to the basic solution as the complexing agents. The solution pH was maintained at about 4.3-4.8 by using NH_4OH. Prior to each deposition, WE was cleaned using alkyl benzene and acetone, and rinsed with DI water. Meanwhile CE was dipped into 30 ml sulfuric acid for 5 s, followed by ultrasonically rinsed with DI water. After the ECD process completed, WE was immediately dried with N_2 gas.

Potentiostat/galvanostat HA-151B and function generator HB-305 (Hokuto Denko) were used in the deposition process and the cyclic voltammetry (CV) measurements. In CV, the potential was swept from 0 V to -1.5 V followed by -1.5 V to 0.5 V and finally from 0.5 V to 0 V at 20 mV/s. Optical in-line transmittance was measured in the range of 300 nm to 1500 nm wavelength using a V-570 UV/VIS/NIR double beam spectrophotometer (JASCO). Film thicknesses were measured via a profile meter Surfcom-1400D (Acrretech-Tokyo Seimitsu). Raman spectra were analyzed by laser Raman spectrophotometer-NRS-3300 (JASCO) using a 632.8 nm red laser as an excitation source. X-ray diffraction (XRD) patterns were recorded by the SmartLab X-ray diffractometer (Rigaku) using a CuKα radiation source. Surface morphology and compositional analysis were conducted using JAMP-9500F field emission

Auger microprobe (JEOL) at a probe voltage of 10 keV and a current of 1 x 10^{-8} A. Scanning electron microscopes (SEM) images were also taken using JAMP-9500F. Photoelectrochemical (PEC) measurements using Xenon lamp (100 mW/cm^2) were conducted in an aqueous electrolyte of 100 mM $Na_2S_2O_3$. The applied voltage was swept at 5 mV/s, and the illumination was mechanically chopped (on and off) for each 5 s.

3. Results and discussion

3.1 Results

Figure 1 illustrates the CV for FeS_xO_y deposition solution with or without complexing agents. All the samples showed clear anodic and cathodic peaks, and during the initial scan from 0 V to about -0.9 V, no visible negative current appeared. The cathodic current started to increase at about -0.9 V. For the control and low concentration of tartaric acid (10 mM) samples, small shifts in the cathodic peaks were observed with a similar cathodic current density and a curve shape. Meanwhile, for high concentration of tartaric acid (50 mM) and lactic acid (56 and 111 mM), even though the curve shape seems similar, a larger negative current density was obtained. Thus, it can be concluded that the negative current was enhanced by addition of high concentration of tartaric acid and lactic acid in the FeS_xO_y deposition solution.

Figure 2 summarizes the thickness measured for the deposited samples. The films were fully covered on the targeted deposited area. Overall, the thickness was increased with addition of the complexing agents. For the deposition with tartaric acid, the thickness was once increased, then decreased at 30 mM, and increased again with increasing concentration. The reason for such oscillation behavior was not understood.

Figures 3 (a)-(f) shows the SEM images for the selected samples. The FeS_xO_y control sample exhibited inhomogeneous grain distribution of various grain sizes. The increase in tartaric acid concentration from 5 mM to 10 mM resulted in homogeneous smaller grain sizes with clear grain boundaries, as shown in Fig. 3 (b) and (c). Similar effects on surface morphology were obtained with increasing lactic acid concentration (Fig. 3 (e)-(f)). Obviously with both acids used as the complexing agents in the solution, the grains size was reduced and the film uniformity was improved.

Auger electron spectroscopy (AES) results for the selected samples are shown in Fig. 4.

S/Fe and O/Fe ratios were calculated using a commercially available standard chemicals FeS and Fe_2O_3 as the reference and are plotted in Figs. 5 (a)-(b). For the FeS_xO_y film deposited with tartaric acid, as shown in Fig. 5 (a), the S/Fe ratio was once decreased and then increased with increasing tartaric acid concentration. Thus there is no clear tendency of increase or decrease in the S/Fe ratio with addition of tartaric acid. The reason for the decrease in S/Fe ratio with low tartaric acid concentration is not understood. The S/Fe ratio is equal to about 2 with some residue amount of oxygen content for the sample with 30 mM tartaric acid. The S/Fe ratio was also almost constant for the films deposited with lactic acid as depicted in Fig. 5 (b) even though the concentration was increased.

On the other hand, the oxygen content in FeS_xO_y film was strongly affected by the complexing agents' concentration. For the tartaric acid samples, as shown in Fig. 5 (a), the O/Fe ratio was significantly reduced at concentrations > 10 mM. Further increase in the concentration up to 50 mM results in further reduction in the oxygen content. For the lactic acid samples also, the O/Fe ratio was greatly reduced when 56 mM lactic acid was added in the deposition solution. However, no further reduction occurred for the concentration greater than 56 mM.

The XRD patterns measured for the selected deposited samples and ITO were shown in Fig. 6. All the observed diffraction peaks are attributed to ITO regardless of the types of complexing agents and the concentration. Thus the deposited films are amorphous, whether the complexing agents were used or not.

Figure 7 represents the Raman spectra for the films deposited under different concentrations of the complexing agents. Raman peaks were formerly reported as follows: pyrite: 336, 341, 373, 377, 425 cm^{-1},[28-29] marcasite: 319, 324, 382 cm^{-1},[28-29] FeS_xO_y: 249, 305 cm^{-1}, and mackinawite ($Fe_{1+x}S$): 208, 256, 298 cm^{-1}.[30] For the measured samples, the $Fe_{1+x}S$ peak appeared only in the control and 56 mM lactic acid samples while no FeS_xO_y phase was observed for low tartaric acid concentration (10 mM). At high concentration of tartaric acid (30-50 mM) and lactic acid (56-111 mM), an additional pyrite peak appeared around 375 cm^{-1}. The largest marcasite peak intensity (326 cm^{-1}) was found for the sample deposited with 50 mM tartaric acid concentration.

Figure 8 illustrates the optical in-line transmittance of the deposited samples. The deposited films with tartaric acid exhibits comparable transmittance to the control sample,

and a clear absorption edge was observed for the control and 30 mM tartaric acid samples. However, no clear absorption edge was detected and lower transmittance (< 2 %) obtained with lactic acid addition. The low transmittance is partly due to the scattering due to the surface roughness.

To estimate the band gap, we plotted $(\alpha h\nu)^2$ and $(\alpha h\nu)^{1/2}$ vs $h\nu$, where α is the absorption coefficient and $h\nu$ is the photon energy. The examples of the plots are shown in Figs. 9 (a)-(b). The plot of $(\alpha h\nu)^{1/2}$ in Fig. 9 (b) does not have a clear straight line portion, while in the plot of $(\alpha h\nu)^2$ as depicted in Fig. 9 (a), the extrapolation of the straight line part seems to intersect the axis in a range of 1−1.2 eV.

Figure 10 depicts the photocurrent response in the PEC measurement for the deposited samples. The weak photoresponse was observed for the control sample, high concentration of tartaric acid (30-50 mM) and lactic acid (56-111 mM) only in negative potential scan. The negative current increased as the sample was illuminated (on), and then decreased as the illumination was interrupted (dark-off). In the PEC measurement, the current due to the minority carrier was enhanced, thus, the results showed that the samples can be classified as p-type.

3.2 Discussion

Complexing agents were normally used to avoid precipitation (e.g., metal hydroxide) by slowing down the release rate of metallic ions in electrolyte solution caused by metal complex formation. In this works, the oxygen content in the deposited films was significantly reduced at high concentration of tartaric acid (> 10 mM) and lactic acid (56-167 mM). Oxygen is probably included in the film initially as $Fe(OH)_2$, and then decomposed into iron oxides. For both complexing agents, free Fe^{2+} ions in the solution would be decreased due to the formation of some iron complex species, which retarded the release of free Fe^{2+} ions and consequently suppressed the formation of $Fe(OH)_2$. Therefore, both complexing agents seem to retard the oxide formation. On the other hand, the film thickness was increased due to the addition of the complexing agents. The deposition in this work is galvanostatic, i.e., the electrical charge supplied was constant for all the depositions. Thus, a part of the current was consumed for reactions other than the sulfide formation without the complexing agents, and the complexing agents suppress such

superfluous reactions and increase the film thickness. In our previous works, it was suggested that tartaric acid enhances the reduction of the sulfur species in ECD of SnS.[27] For FeS_xO_y, although the S/Fe ratio did not increase significantly, the complexing agents are considered to enhance the reduction of the sulfur species and the sulfide formation, which resulted in the increase in the film thickness.

The addition of the complexing agents also results in higher marcasite peaks intensity in the Raman spectra. In addition, lactic acid presence in the solution results in poor transmittance which is less than 2 %. This lower transmittance is partly due to the larger film thickness and partly associated with the defects states causing below-band-gap absorption and/or the marcasite phase, having a much smaller band gap. In PEC measurement, the improvement of the photoresponse was not observed for the samples deposited with the complexing agents. Thus, although the composition became more stoichiometric due to the addition of the complexing agents with the oxygen content much reduced, the optical and electrical properties do not seem to be improved significantly. In other words, the properties of amorphous iron sulfide are not seriously deteriorated by the introduction of oxygen. It was shown on the basis of Mössbauer study that Fe atoms are coordinated to six anions (S or O) in ECD-deposited amorphous FeS_xO_y, as in crystalline FeS_2.[31] Thus, in spite of the dissimilarity of iron sulfides and iron oxides, sulfur and oxygen seem to play a similar anion role in amorphous FeS_xO_y. As a result, its properties are not drastically influenced by the oxygen content.

In future study, the heterostructures with an n-type semiconductor such as ZnO will be fabricated using FeS_xO_y films deposited with the complexing agents, and the effects of film composition (oxygen content) on the junction properties will be discussed.

4. Conclusions

FeS_xO_y thin films were deposited on ITO-coated glass substrates via galvanostatic ECD from an aqueous of solution containing $Na_2S_2O_3$ and $FeSO_4$ with controlled pH, and the effects of different concentration of tartaric acid and lactic acid were studied. With the addition of complexing agents, the thickness was increased, and the O/Fe ratio was decreased. However, no significant effects were found for photoresponse and crystallinity. Thus, oxygen atoms do not seem to significantly affect the properties of amorphous iron

sulfide films, probably because the local bonding configuration around Fe atoms is not altered by substitution of sulfur with oxygen. The reduction of oxygen content in the FeS_xO_y film can be explained by considering the suppression of $Fe(OH)_2$ formation.

References

1) S. Kawai, R. Yamazaki, S. Sobue, E. Okuno, M. Ichimura, APL Mater., **2**, 032110-1 (2014).
2) Y. Bi, Y. Yuan, C.L. Exstrom, S.A. Darveau, J. Huang, Nano Lett., **11**, 4953 (2011).
3) S. Nakamura, A. Yamamoto, Sol. Energy Mater. Sol. Cells, **65**, 79 (2001).
4) A. Ennaoui, S. Fiechter, W. Jaegermann, H. Tributsch, J. Electrochem. Soc., **133**, 97 (1986).
5) A. Ennaoui, S. Fiechter, C. Pettenkofer, N. Alonso-Vante, K. Büker, M. Bronold, C. Höpfner, H. Tributsch, Sol. Energy Mater. Sol. Cells, **29**, 289 (1993).
6) I.J. Ferrer, D.M. Nevskaia, C. de las Heras, C. Sánchez, Solid State Commun., **74**, 913 (1990).
7) A. Ennaoui, S. Fiechter, H. Goslowsky, H. Tributsch, J. Electrochem. Soc., **132**, 1579 (1985).
8) A. Yamamoto, M. Nakamura, A. Seki, E. Li, A. Hashimoto, S. Nakamura, Sol. Energy Mater. Sol. Cells, **75**, 451 (2003).
9) R.H. Misho, W.A. Murad, Sol. Energy Mater. Sol. Cells, **27**, 335 (1992).
10) L. Meng, J.P. Tu, M.S. Liu, Mater. Lett., **38**, 103 (1999).
11) I.J. Ferrer, C. Sánchez, J. Appl. Phys., **70**, 2641 (1991).
12) G. Willeke, R. Dasbach, B. Sailer, E. Bucher, Thin Solid Films, **213**, 271 (1992).
13) D. Lichtenberger, K. Ellmer, R. Schieck, S. Fiechter, Appl. Surf. Sci., **70**, 583 (1993).
14) G. Chatzitheodorou, S. Fiechter, R. Könenkamp, M. Kunst, W. Jaegermann, H. Tributsch, Mater. Res. Bull., **21**, 1481 (1986).
15) C. Höpfner, K. Ellmer, A. Ennaoui, C. Pettenkofer, S. Fiechter, H. Tributsch, J. Cryst. Growth, **151**, 325 (1995).
16) D.A. Mazón-Montijo, M.T.S. Nair, P.K. Nair, ECS J. Solid State Sci. Technol., **2**, P465 (2013).
17) L. Huang, F. Wang, Z. Luan, L. Meng, Mater. Lett., **64**, 2612 (2010).
18) H. Siyu, L. Xinyu, L. QingYu, C. Jun, J. Alloys Compd., **472**, L9 (2009).
19) K. Yang, S. Kawai, M. Ichimura, Thin Solid Films, **573**, 1 (2014).
20) A.S. Aricò, V. Antonucci, P.L. Antonucci, E. Modica, S. Ferrara, N. Giordano, Mater. Lett., **13**, 12 (1992).
21) A. Gomes, H.M. Mendonça, I.M. da Silva Pereira, M.A.F. Costa, J. Solid State Electrochem., **4**, 168 (2000).
22) A. Vedavathi, K. Ramakrishna Reddy, Y. Munikrishna Reddy, IOSR-JEN, **05**, 65 (2015).

23) A. Kassim, H.S. Min, L.Y. Yee, T.W. Tee, S. Nagalingam, Can. J. Pure Appl. Sci., **6**, 1863 (2012).
24) K. Manikandan, P. Mani, C. Surendra Dilip, S. Valli, P. Fermi Hilbert Inbaraj, J. Joseph Prince, Appl. Surf. Sci., **288**, 76 (2014).
25) F. Kang, M. Ichimura, Thin Solid Films, **519**, 725 (2010).
26) J.R. Brownson, C. Georges, G. Larramona, A. Jacob, B. Delatouche, C. Lévy-Clément, J. Electrochem. Soc., **155**, D40 (2008).
27) A. Supee, Y. Tanaka, M. Ichimura, Mater. Sci. Semicond. Process., **38**, 290 (2015).
28) M. Umehara, Y. Takeda, H. Azuma, T. Motohiro, Jpn. J. Appl. Phys., **51**, 02BP10-1 (2012).
29) R. Morrish, R. Silverstein, C.A. Wolden, J. Am. Chem. Soc., **134**, 17854 (2012).
30) J.A. Bourdoiseau, M. Jeannin, R. Sabot, C. Rémazeilles, P. Refait, Corros. Sci., **50**, 3247 (2008).
31) M. Ichimura, T. Kajima, S. Kawai, K. Mibu, Jpn. J. Appl. Phys., **55**, 038006-1 (2016).

Figure Captions

Fig. 1. (Color online) Cyclic voltammetry (CV) for the solutions with and without the complexing agents, tartaric acid (T. acid), and lactic acid (L. acid).

Fig. 2. (Black and white) Thickness of the deposited films as a function of the complexing agent concentration. (a): tartaric acid (T. acid), and (b): lactic acid (L. acid).

Fig. 3. (Color online) SEM images for the selected deposited samples (Scale bar: 4μm, x5000). (a): control FeS_xO_y, (b): tartaric acid 5 mM, (c): tartaric acid 10 mM, (d): tartaric acid 30 mM, (e): lactic acid 56 mM, and (f): lactic acid 111 mM.

Fig. 4. (Color online) AES spectrum for the selected samples. (a): control FeS_xO_y, (b): tartaric acid 30 mM, and (c): lactic acid 56 mM.

Fig. 5. (Black and white) Compositional analysis by AES for the deposited samples under different concentrations of the complexing agents. (a): tartaric acid (T. acid), and (b): lactic acid (L. acid).

Fig. 6. (Color online) XRD patterns for the selected deposited samples. (a): ITO, (b): control FeS_xO_y, (c): tartaric acid 5 mM, (d): tartaric acid 10 mM, (e): tartaric acid 30 mM, (f): lactic acid 56 mM, and (g): lactic acid 111 mM.

Fig. 7. (Color online) Raman spectra for the deposited samples (a): control FeS_xO_y, (b): tartaric acid 10 mM, (c): tartaric acid 30 mM, (d): tartaric acid 50 mM, (e): lactic acid 56 mM, and (f): lactic acid 111 mM.

Fig. 8. (Color online) Optical in-line transmittance of the deposited samples. (a): control FeS_xO_y, (b): tartaric acid 10 mM, (c): tartaric acid 30 mM, (d): lactic acid 56 mM, and (e): lactic acid 111 mM.

Fig. 9. (Color online) Plots of (a) $(\alpha h\nu)^2$ and (b) $(\alpha h\nu)^{1/2}$ versus $h\nu$ for the deposited samples.

Fig. 10. (Color online) Photocurrent responses in the PEC measurement for the control sample, and the samples deposited with tartaric acid (T. acid), and lactic acid (L. acid).

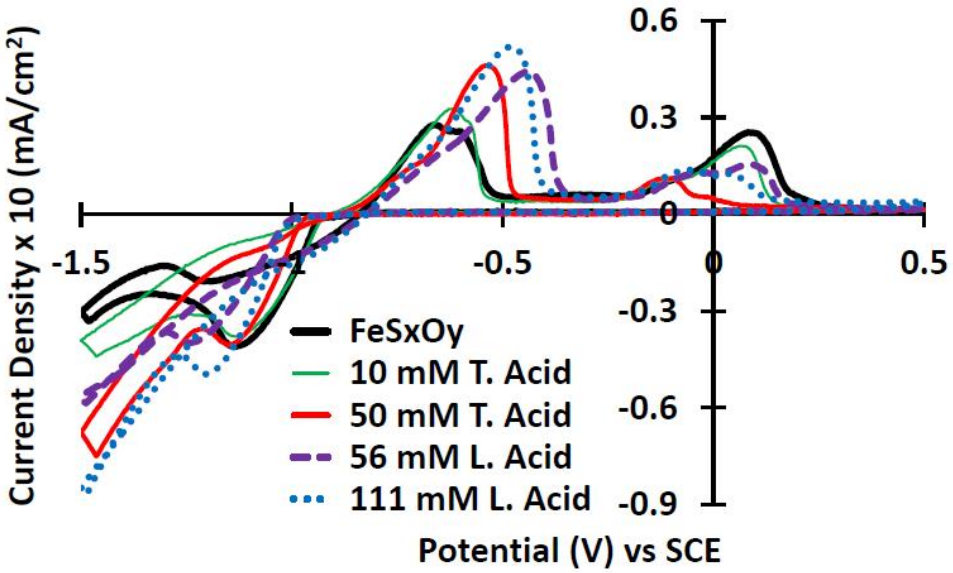

Fig. 1. (Color online)

Black and white print

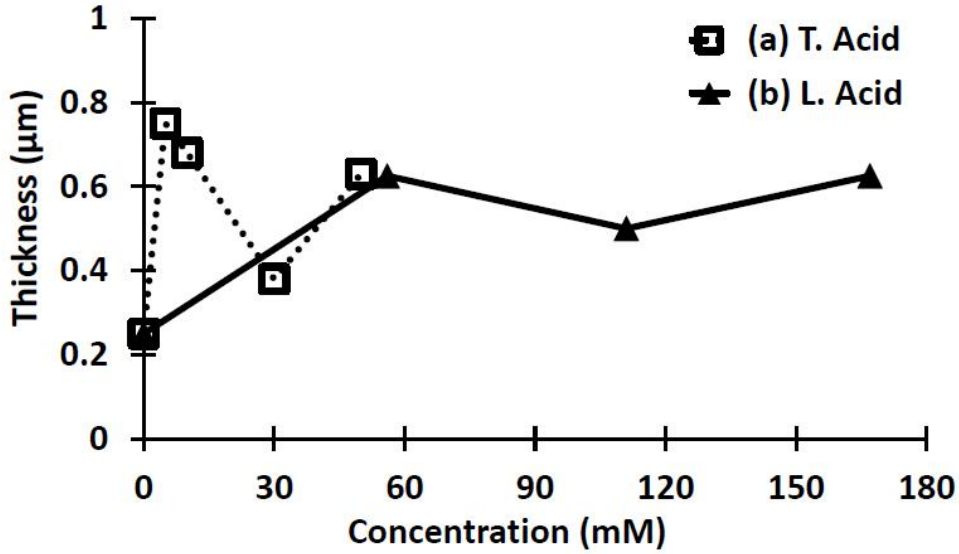

Fig. 2. (Black and white)

Black and white print

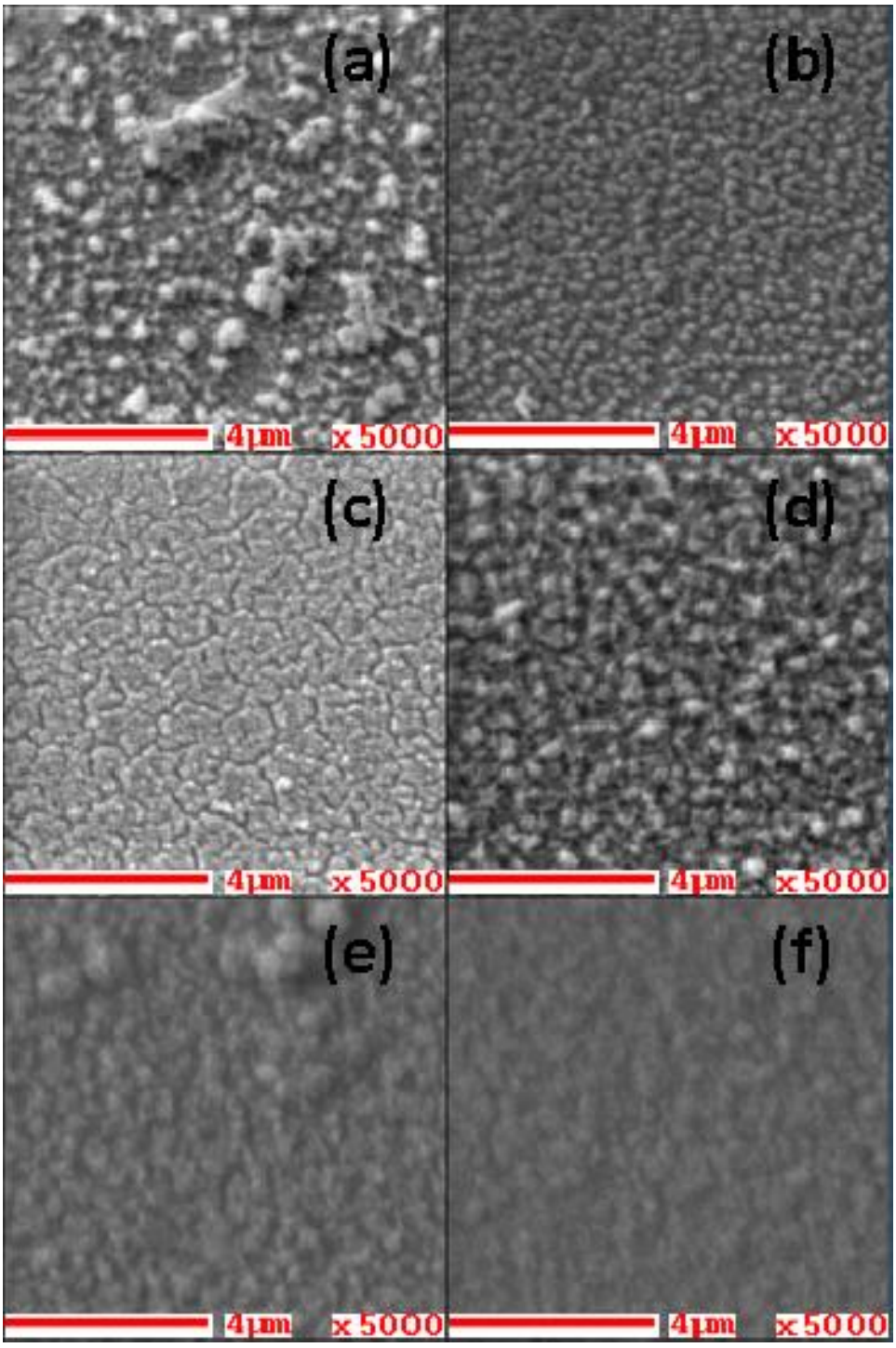

Fig. 3. (Color online)

Black and white print

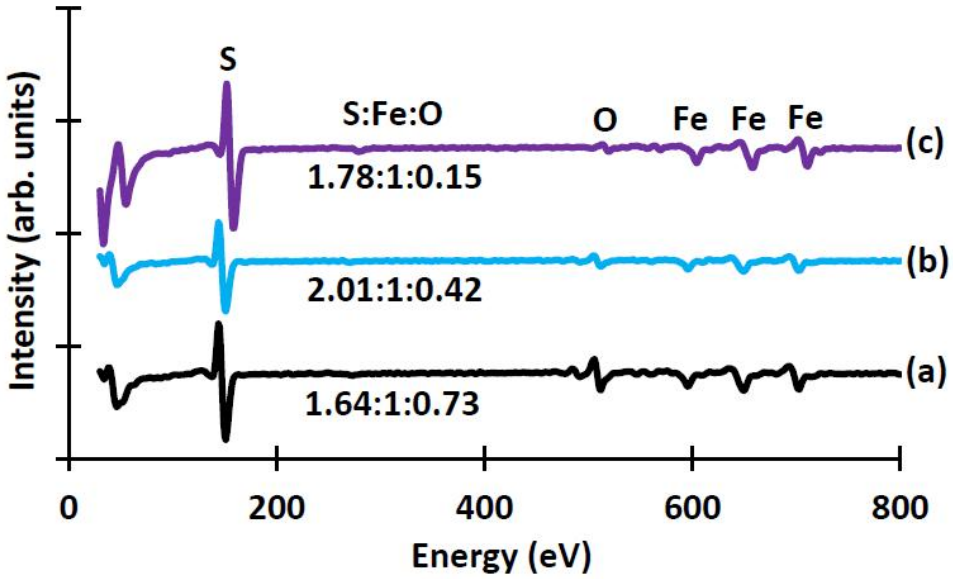

Fig. 4. (Color online)

Black and white print

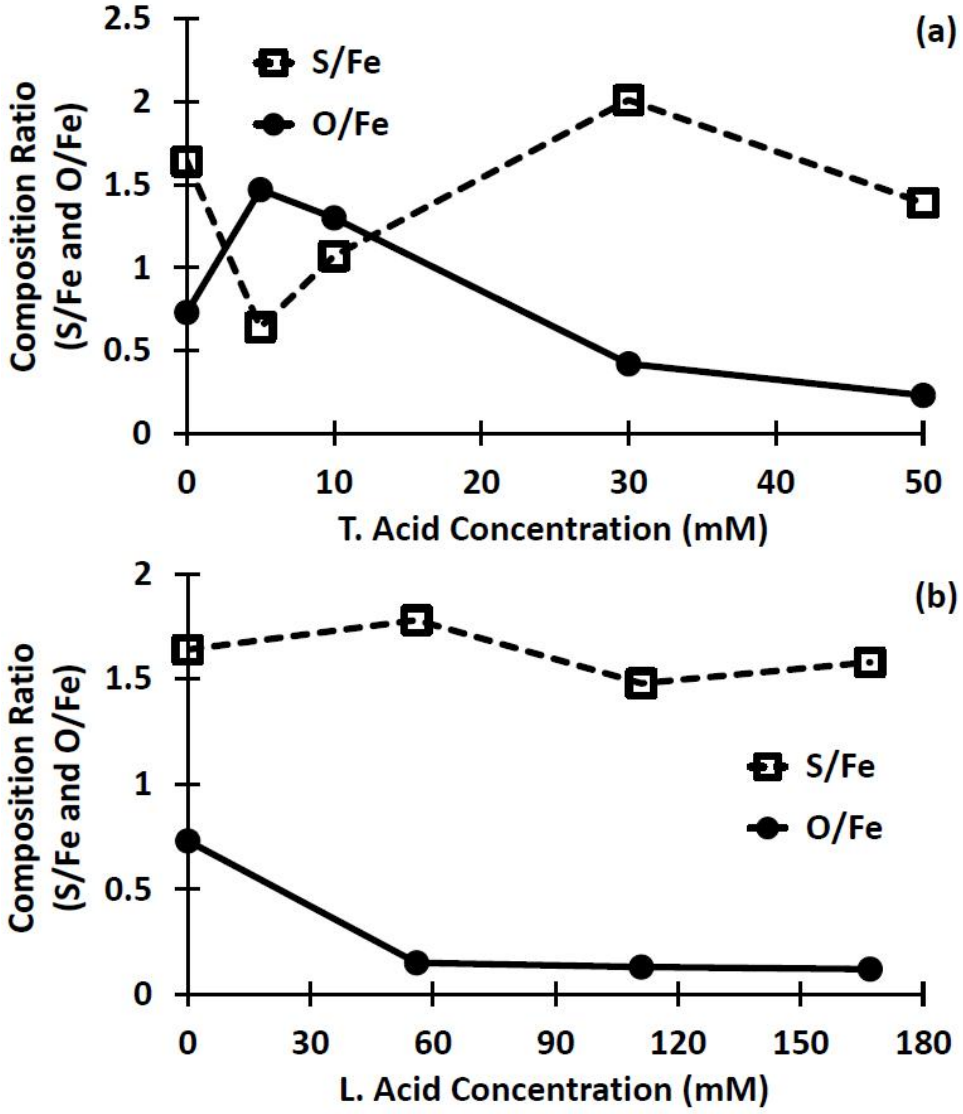

Fig. 5. (Black and white)

Black and white print

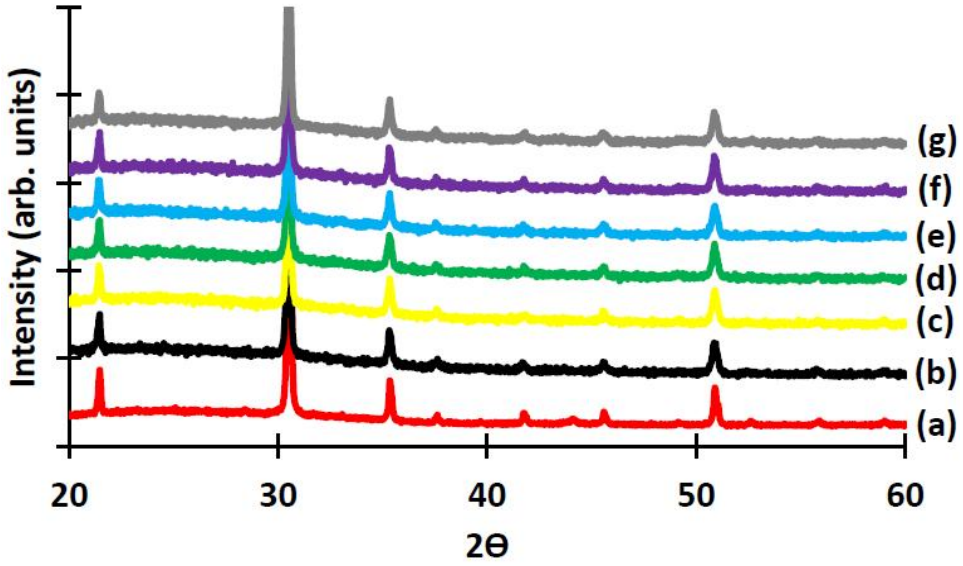

Fig. 6. (Color online)

Black and white print

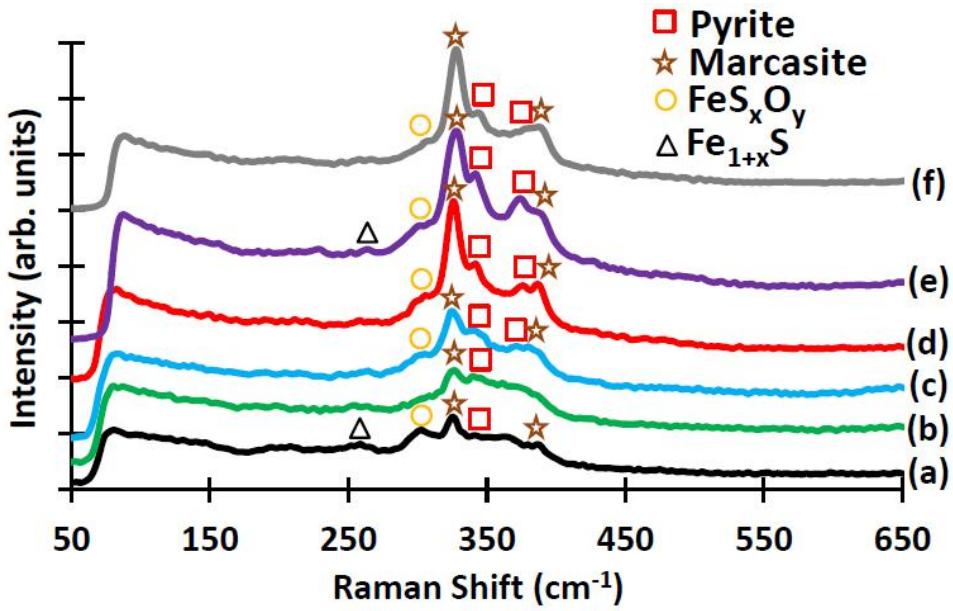

Fig. 7. (Color online)

Black and white print

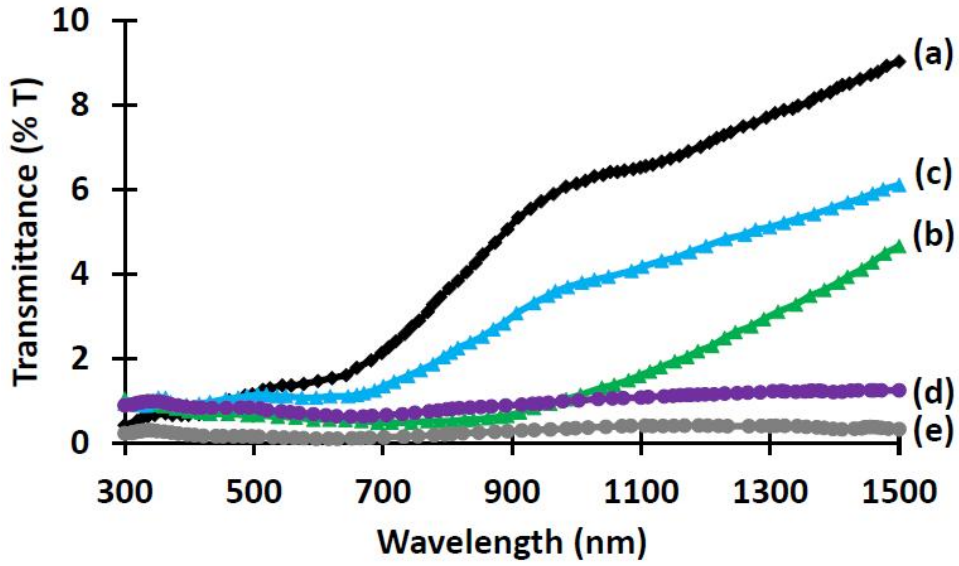

Fig. 8. (Color online)

Black and white print

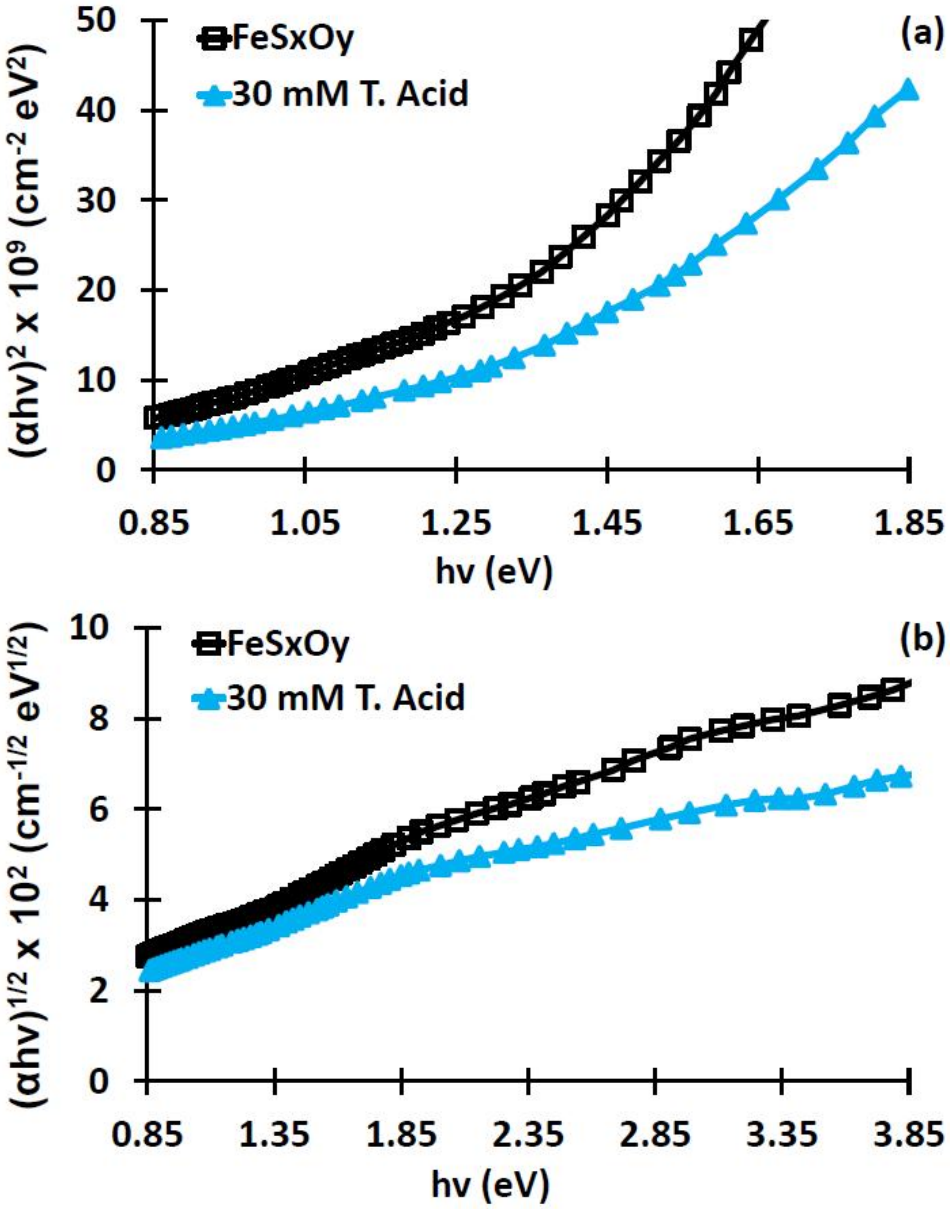

Fig. 9. (Color online)

Black and white print

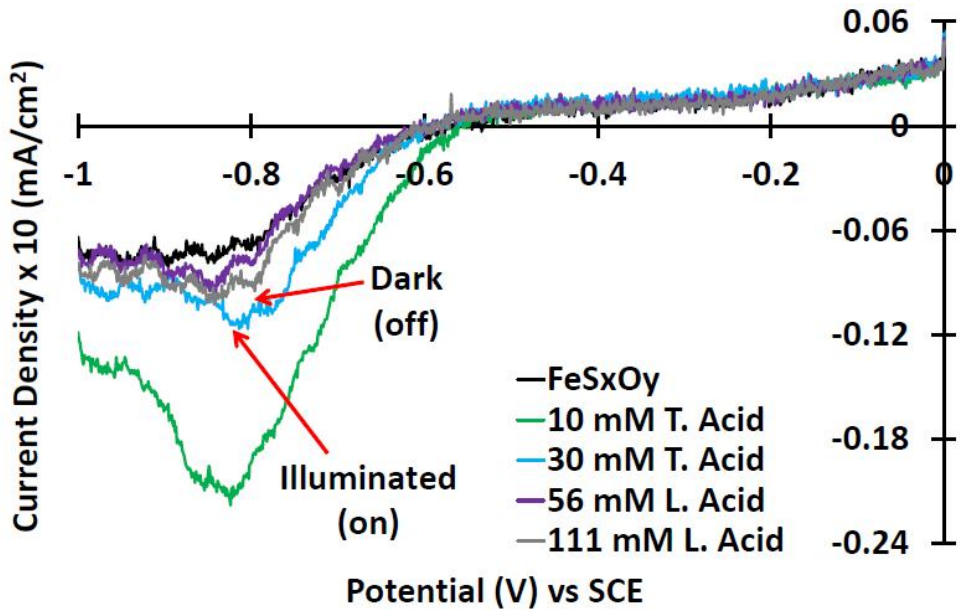

Fig. 10. (Color online)

Black and white print